JOURNAL OF SPACECRAFT AND ROCKETS
Vol. 32, No. 6, November–December 1995

Rotating Nose Tip Effects on Slender Body Aerodynamics at High Angles of Attack

R. D. Maynes* and G. A. Gebert†
Utah State University, Logan, Utah 84322

An array of experiments have been conducted on a finless, slender body with a rotating nose tip having up to three nose tip strakes. The model had a fineness ratio of 20.0 and a 2.7 tangent ogive nose. The experiments were performed at a Mach number of 0.15 and a Reynolds number of 9.93×10^5. The results show that the use of a rotating nose tip on a slender body can significantly reduce (up to 80%) the out-of-plane loading on the body. The amount of reduction is dependent upon the rotation rate and the number of strakes on the rotating nose. As the number of strakes increased, the effect of the rotation rate became less evident. The results show that a reduction in the side force did not necessarily coincide with a corresponding reduction of the yawing moment. In virtually all cases, the spinning tip worked best in reducing the out-of-plane loading below some critical angle of attack where the flow appears to behave with a convective instability. Tests above the critical angle of attack showed less dependence on the effects of the nose tip disturbances. These effects argue that above this critical angle the flow is controlled by an absolute instability.

Nomenclature

CLN	= yawing moment coefficient, $N/(q_\infty SD)$
CY	= side force coefficient, $Y/(q_\infty S)$
D	= diameter of body, in.
L	= length of entire body, in.
L/D	= fineness ratio
M	= Mach number
N	= yawing moment, in.-lbf
q_∞	= upstream dynamic pressure, lbf/in.^{2}
Re	= Reynolds number
S	= body cross-sectional area, in.^{2}
x	= axial body-fixed coordinate
Y	= side force, lbf
y	= body-fixed coordinate
z	= body-fixed coordinate
α	= angle of attack
ϕ	= roll angle
ω	= rotation rate, rpm

Subscript

∞	= freestream conditions

Introduction

WITH the constant development of more highly maneuverable aircraft, there has been a significant amount of interest in the flight of slender bodies (missiles) at high angles of attack. A great many experimental and analytical investigations have been conducted in this area. Analyses through the 1950s to the mid-1970s largely focused on the impulse analogy, which describes the development of the wake along the body in terms of the flow behind a two-dimensional fluid started impulsively from rest.[1,2] Since that time, some of the topics that have been researched are the vortex wake and development,[3] flow visualization studies of the vortex structure,[4] pressure and flowfield distribution,[5] methods for predicting the aerodynamic forces,[6–10] mechanisms for alleviating the out-of-plane loads,[11–14] and the nature of the instability causing asymmetric flow.[15–19] However, most of the previous research has focused on forebodies or finless bodies with fineness ratios (L/D) less than 10.0.

For the aerodynamics on slender axisymmetric bodies, in the angle-of-attack range of 0–90 deg, there are at least four distinct regimes. At very low angles of attack (less than 5 deg), there is no discernible boundary-layer separation, and the flow can be characterized by a classical potential flowfield with an attached laminar or turbulent boundary layer. At these small angles of attack, the dominant forces and moments a body experiences are the in-plane aerodynamics. Linear theory generally estimates the aerodynamics with reasonable accuracy.

As the angle of attack increases (5–20 deg), the boundary layer begins to separate from the body, and the separated flow region moves forward with increasing angle of attack. In this range of angle of attack, the flow on the leeward side of the body separates and rolls up into regions of concentrated vorticity. These regions of vorticity are steady, symmetric, and counter-rotating. They induce a vortex lift and have only a slight effect on the out-of-plane loading. In this region linear inviscid theory becomes inapplicable, and accurate aerodynamic predictions require the inclusion of viscous theory.

At some critical angle of attack (approximately 15–20 deg), the flow separating off the leeside of the body rolls up into a pair of steady asymmetric vortices (Fig. 1). This flow structure remains for the angles of attack from 20 to 70 deg. When viewed in cross section, the vortex structure resembles a von Kármán vortex street. As a result of the asymmetric vortex formation, large side forces, yawing moments, and dynamic out-of-plane loading may occur due to the velocity induced by the vortex-dominated wake. Finally, as the angle of attack approaches 90 deg (70–90 deg), the flowfield is similar to that of the unsteady flow occurring around an infinite right circular cylinder.

For the work reported in this paper, the aerodynamics of interest are the out-of-plane aerodynamics, meaning the side force and yawing moment. The in-plane aerodynamics, normal force and pitching moment, are affected by the asymmetric vortex structure, but not nearly to the extent of the out-of-plane loads.

Present Interest

The range of interest for this paper is the range associated with the asymmetric vortices (approximately 15–20 deg). Wind-tunnel investigators have shown that a large variety of vortex flows may be encountered, depending on the angle of attack, particular flow conditions, and body geometry.[22,23] At some given high angle of attack, the asymmetric vortices may set up in the configuration shown in Fig. 1. This vortex formation will remain steady until some condition

Received Nov. 28, 1994; revision received May 25, 1995; accepted for publication June 6, 1995.

*Research Assistant, Department of Mechanical and Aerospace Engineering. Student Member AIAA.

†Assistant Professor, Department of Mechanical and Aerospace Engineering. Member AIAA.

changes, such as a small disturbance in the upstream flow. At that point, the separated flow may change and set up a vortex formation in a different configuration, causing the loading to be different even with the same flight condition. Because of this attribute it is very difficult to predict the actual out-of-plane aerodynamic loading on a body, since for any given condition the values are not uniquely determined. The out-of-plane loads can be very large and thus devastating to the flight and control of a slender body.

Since the out-of-plane loads are extremely sensitive to factors that are difficult to control and predicting is very difficult, recent research has focused on methods of eliminating the out-of-plane loads. Investigators[13,21] have concluded that minute model irregularities in the nose tip region control the vortex asymmetry. Geometric perturbations, such as nose bluntness,[21] strakes,[11] boundary-layer trips,[13] spinning nose tips,[11,13] and combinations of the aforementioned, have been tried as a means to control the flow asymmetry. All of these investigations showed a reduction in the side force, and some were significant. However, most of the previous investigations have focused only on nose tips or on bodies with fineness ratios less than 10.

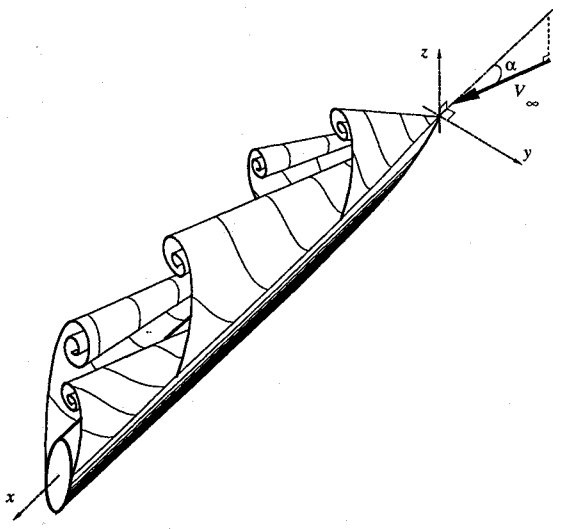

Fig. 1 Schematic of a finless body at a high angle of attack with asymmetric vortex shedding.

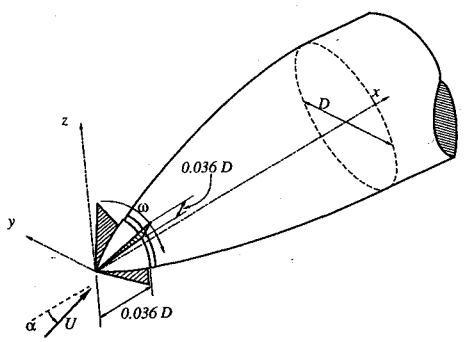

Fig. 2 Schematic of a rotating nose tip with strakes to induce vorticity.

The focus of this paper is to present the results of a wind-tunnel investigation on a slender body with a rotating nose tip with and without strakes. The body used for the investigation is a finless model of the AMRAAM missile. The length to diameter ratio L/D is 20. Located on the nose tip are small strakes that act to perturb the flow and thus induce vorticity into the flow. As this nose tip, with the strakes, rotates about the axis of the body, Fig. 2, vortices are continuously shed on one side or the other, causing the flow to be unsteady. The alternating shed vortices are expected to be of nearly equal strength. Thus, the forces that are induced due to these vortices should cancel each other out over a time average. If not, a complete cancellation and reduction would occur, and the direction the side force acts should become more predictable. Previous investigations[20] include tests of a finless body without a rotating nose tip. The results from the rotating tip results are compared with these baseline cases to show the effects of a rotating tip.

Experimental Arrangement

The experiments were conducted in one of Utah State University's wind tunnels. The tunnel is a low-speed tunnel with a test section of 4.0 × 4.0 ft. The tunnel speed can be varied from 0 to 200 ft/s. All tests were conducted at a Mach number of 0.15 and a Reynolds number based on the diameter of the body of 9.93×10^5. The airspeed was measured by a pitot tube and manometer with an accuracy of ±0.05 in. of water. The model was mounted to a solid linkage sting by a strain gauge force-torque sensor. The sensor was accurate to 1.25% of full load capacity of the sensor. The full load capacity was 8 lbf in the normal and side force directions, 10 lbf in axial force, 84 in.-lbf for the pitching and yawing moments, and 15 in.-lbf for the rolling moment. The angle of attack was swept from −10 to 70 deg with the solid linkage being varied by a linear actuator. The actuator moved a rack along a pinion that changed the angle of attack. Figure 3 shows a schematic of the model and sting system. Because of the mounting method the axial force for the experiments was not expected to be accurate, and it was not measured.

The JR3 force-torque sensor is a strain gauge device that outputs voltages to a data acquisition system (DAS). The DAS used for the tests was a 386, 25 MHz computer with a PCL 812 data acquisition card. The system was able to take samples at a rate of over 1000 samples/s (Hz). For the tests the sampling rate was 50 Hz/channel with all six channels being sampled. In comparison with results sampled at 1000 Hz the results were almost identical. These comparisons were made for all channels and the results were all similar.

A fast Fourier transform (FFT) was done on the data from the sensor that showed the frequency range of maximum spectral energy. This critical frequency range was well within the sampling rate and below the cutoff value of the JR3 cutoff filter. Thus, it was determined that the signal was not biased or in error. The raw data are presented in this paper.

For the experimental program, a scaled model of the AMRAAM missile without fins was used. The geometry is shown schematically in Fig. 4. The diameter of the model D was 1 in. The fineness ratio of the body was 20, and the ogive nose had a length of $2.7D$. The moment reference center was taken along the body central axis at a distance of $10.2D$ from the nose tip. A small ±12-V dc motor was mounted in the nose section of the model. The motor, which rotated the nose tip, had a varying speed from 200–10,000 rpm. Nose tips

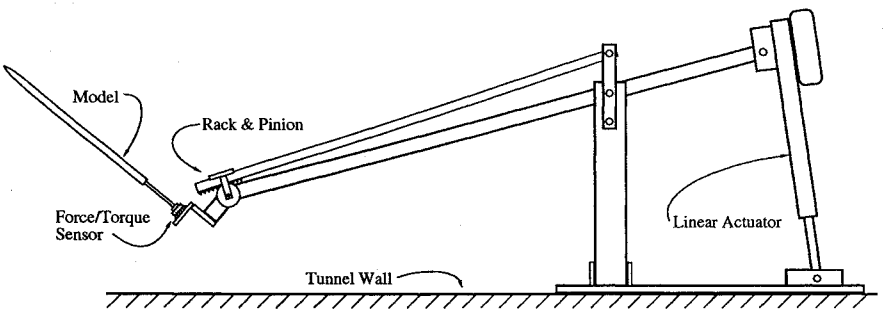

Fig. 3 Model mounted on sting with the force/torque sensor.

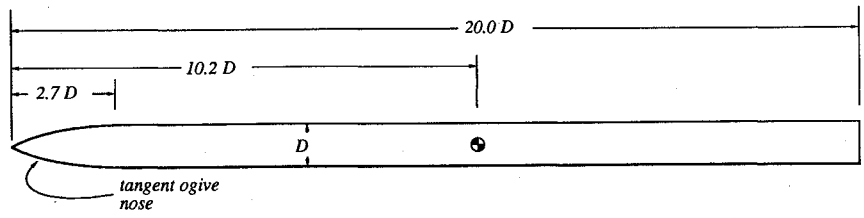

Fig. 4 Schematic of the slender body test model.

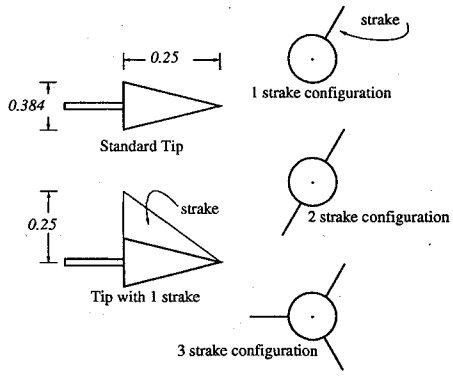

Fig. 5 Schematic of nose tip/strake geometry (dimensions in inches).

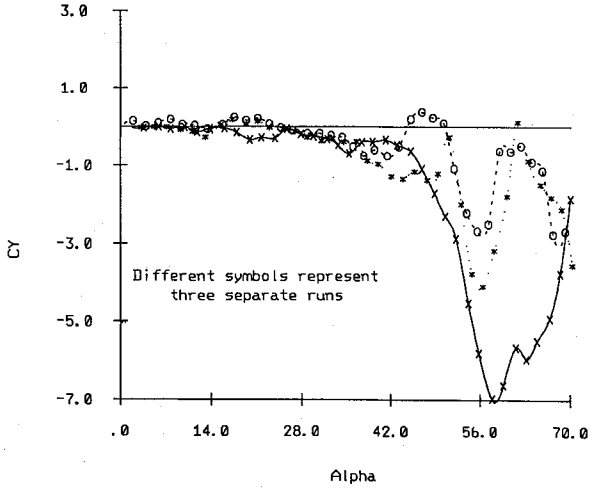

Fig. 6 Side force coefficient for a finless body, with a nonrotating nose and no strakes.

were easily exchanged and mounted on the body. The nose tips used had up to three strakes mounted on them. Schematics of the nose tips are shown in Fig. 5.

Body-Alone Results with No Strakes or Rotations

Experiments for a nonrotating body without fins are reported in Ref. 20 and are used for comparison with the present study. Figures 5 and 6 show the side force and yawing moment coefficients, respectively, for a finless body without a rotating nose tip. Three separate runs were conducted at the same flow conditions for the baseline results and are all shown on the baseline figures.

Figure 6 shows that the side force is reasonably close to zero up to about 40-deg angle of attack, above which the magnitude of the side force coefficient increases significantly. The three separate runs were conducted with the same upstream flow conditions and model roll angle. Apparently, small disturbances in the flowfield caused different asymmetric vortex formations resulting in significantly different out-of-plane loading, especially above 40 deg. This result emphasizes the unpredictability of the loadings at any given flow condition. Interestingly, as noted in Ref. 20, the data that show the largest side force also show the smallest yawing moment (Fig. 7).

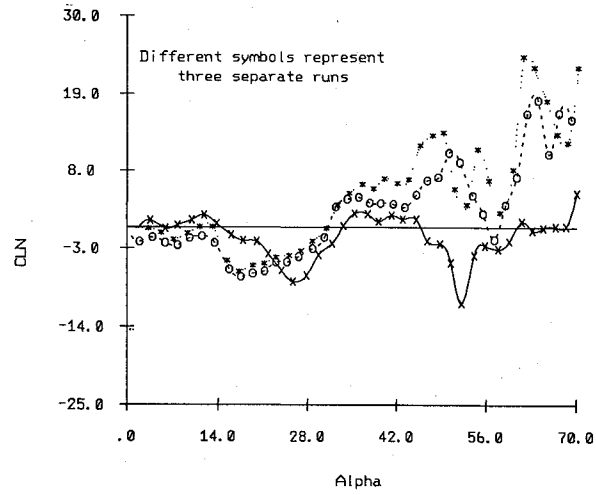

Fig. 7 Yawing moment coefficient for a finless body, with a nonrotating nose and no strakes.

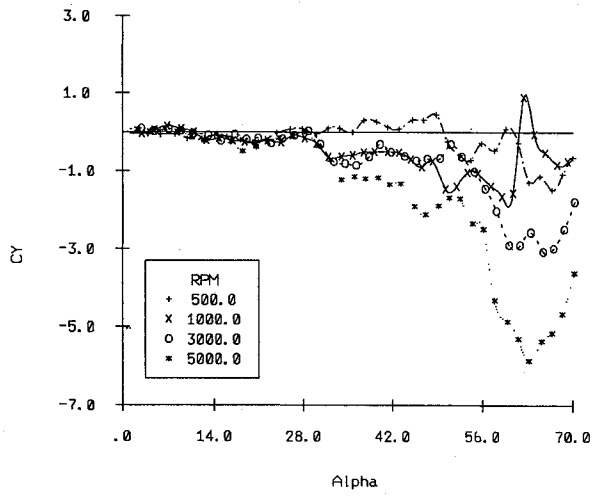

Fig. 8 Side force coefficient for finless body without strakes on a counterclockwise rotating nose tip.

Rotating Nose Tip Results

Tests were conducted at a variety of nose tip rotation rates and four different nose tip configurations. Except for the single strake case, the fins were always oriented to give an axisymmetric configuration as shown in Fig. 5. The following are the results for the various nose tips.

Nose Tip Without Strakes

Figures 8 and 9 correspond to the slender body with a counterclockwise rotating nose tip without strakes. For the side force (Fig. 8), the case with the nose tip rotating at 500 rpm shows the most significant reduction in the loading up to about 50 deg. The 1000 and 3000 rpm cases show little difference from the baseline (Fig. 6) up to 50 deg. Above 50 deg, the 500 and 1000 rpm cases show a significant reduction from all of the baseline cases. The 5000 rpm case seems to induce an increased side force, and the 3000 rpm case shows behavior similar to the baseline cases.

The yawing moment (Fig. 9) shows little difference between the rotating nose tip without fins case and the baseline case. However,

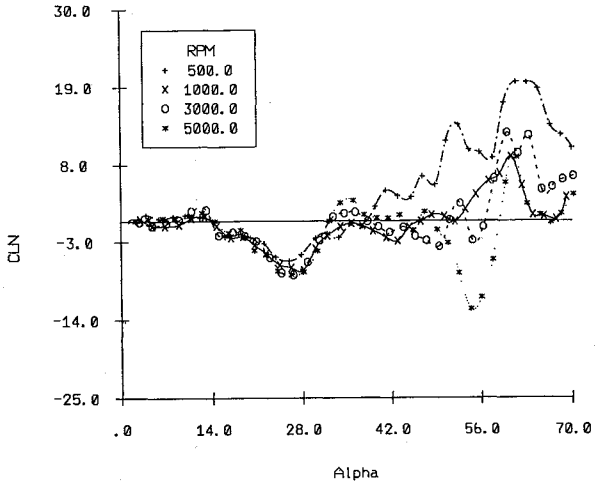

Fig. 9 Yawing moment coefficient for a finless body without strakes on a counterclockwise rotating nose tip.

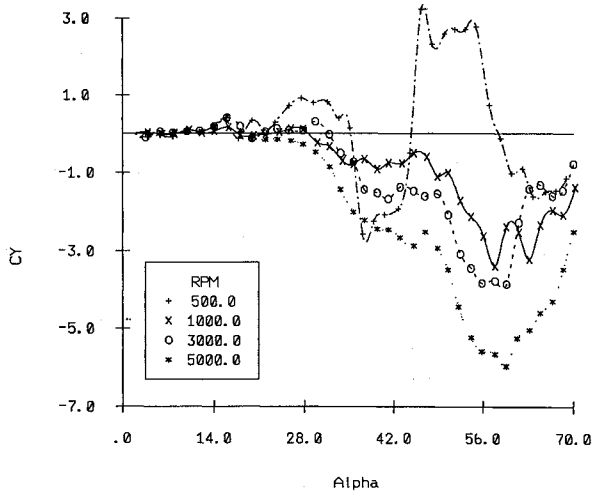

Fig. 10 Side force coefficient for a finless body with one strake on a counterclockwise rotating nose tip.

some items of interest can be seen by looking at the side force graph and the yawing moment graph together. Up to about 30 deg all of the plots have quite similar behavior. At approximately 15 deg, there is a dip towards the negative for all plots on the yawing moment graph. The side force graph shows no corresponding dip in the data. This trend continues up to about 30 deg. This result seems to indicate that the yawing moments at these angles are generated by a relatively small side force located close to either the tip or the tail of the body, or both.

As the angle of attack increases from 40 to 70 deg, there are significant changes in the out-of-plane loading. The 500 rpm case, which showed the greatest reduction in side force for $\alpha < 40$ deg, produces the largest yawing moment, and the 5000 rpm case, which gave the largest side force, has a corresponding yawing moment that is reasonably small. The 500 rpm case can be explained again by having a small side force close to the tail of the body. However, to have a large side force and a small yawing moment, the force must act closely to the center of gravity or be distributed along the body.

One Strake

Figures 10–13 show results with one strake on the nose tip. Figures 10 and 12 show the side force for a counterclockwise and a clockwise rotating tip, respectively. These figures indicate that a significant reduction in the side force did not occur. However, all curves follow similar trends. One trend in the data demonstrates that as the rotation rate increases, past 1000 rpm, the side force gets larger. The 500 rpm case does not show any significant side force reduction. Both the counterclockwise and the clockwise rotations

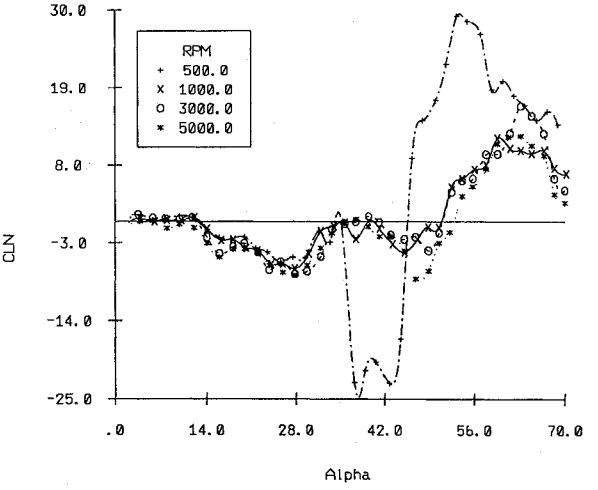

Fig. 11 Yawing moment coefficient for a finless body with one strake on a clockwise rotating nose tip.

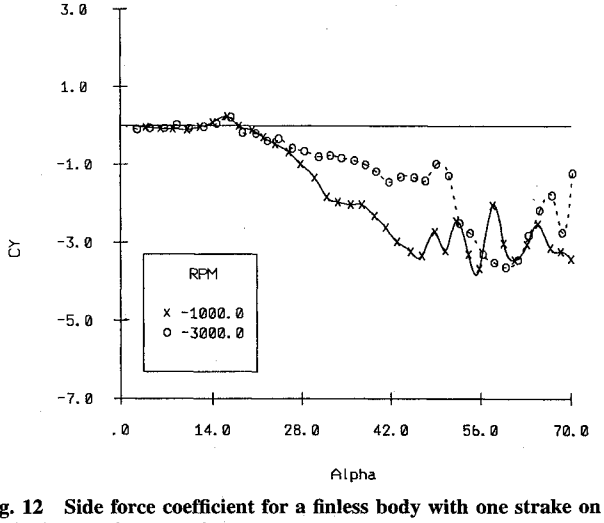

Fig. 12 Side force coefficient for a finless body with one strake on a clockwise rotating nose tip.

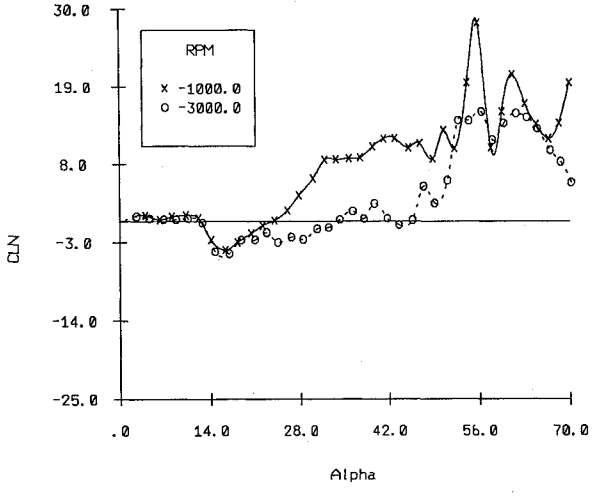

Fig. 13 Yawing moment coefficient for a finless body with one strake on a clockwise rotating nose tip.

for the 1000 and 3000 rpm cases give similar results. One difference is that for the clockwise rotation the initial formation of a side force occurs at a lower angle of attack than for the counterclockwise cases. It was expected that the rotation direction would bias the out-of-plane loading. However, this result was not observed from Figs. 10 and 12. The side force formed on the same side regardless of the rotation rate. The reason for this may be that the flow in the tunnel or the model has some imperfection, which generates

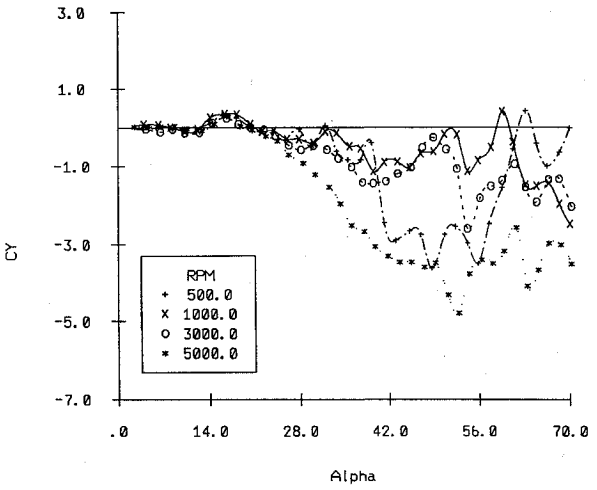

Fig. 14 Side force coefficient for a finless body with two strakes on a counterclockwise rotating nose tip.

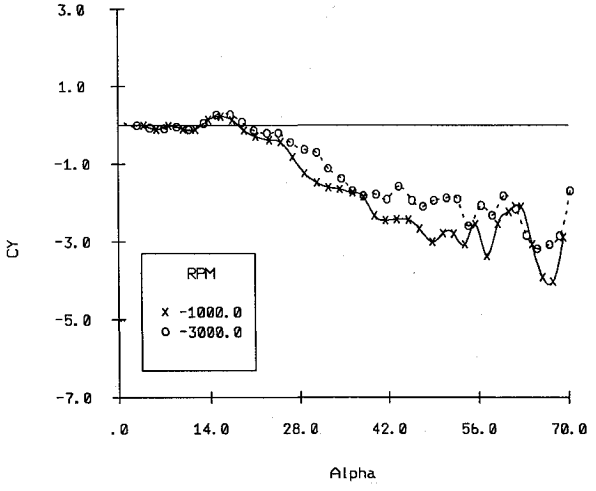

Fig. 16 Side force coefficient for a finless body with two strakes on a clockwise rotating nose tip.

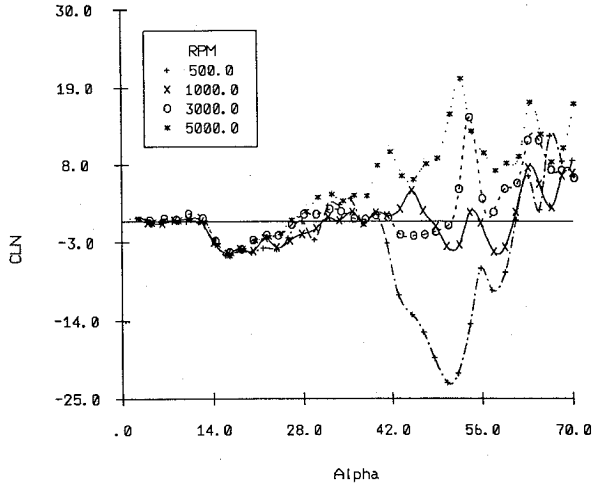

Fig. 15 Yawing moment coefficient for a finless body with two strakes on a counterclockwise rotating nose tip.

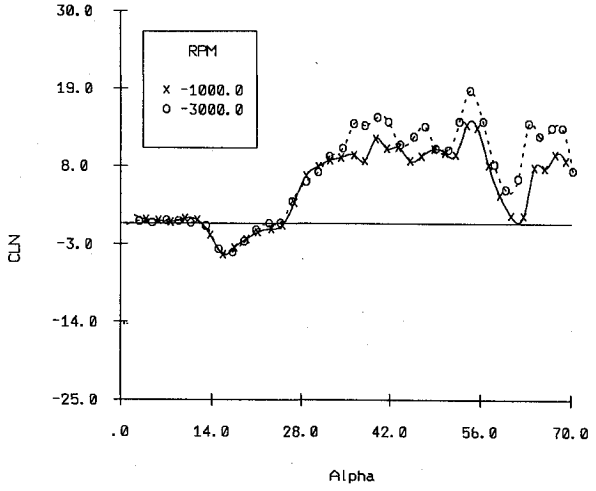

Fig. 17 Yawing moment coefficient for a finless body with two strakes on a clockwise rotating nose tip.

a tendency of the side force to always form in the same direction. Apparently, the rotating nose tip cannot always overcome this effect.

Figure 11 shows that for the 1000, 3000, and 5000 rpm cases there is nearly a 50% reduction from the baseline yawing moment coefficients for a large range of angle of attack. The yawing moment with a 500 rpm rotation rate shows similar behavior as the side force. It shows good reduction from the baseline only up to $\alpha = 20$ deg. In general, the yawing moment curves do not follow the characteristics of their corresponding side force curves. For the clockwise rotating nose tip, Fig. 13 shows that the yawing moment has a strong coupling with the side force. The magnitude for this case is of similar magnitude as the baseline cases.

Two Strakes

The results for a rotating nose tip with two strakes (Figs. 14–17) are similar to those of one strake. For the counterclockwise rotation, the magnitude of the side forces for the two-strake cases are smaller at all rotation rates than for the one-strake case. Similarly, as for the one-fin results, the 1000 and 300 rpm cases show the most significant reduction of the side force and not the yawing moment. The 1000 rpm case shows the most significant reduction of about 50% from the baseline at angles of attack above 40 deg. For the two nose strakes, the 500 rpm case does show some side force reduction. This result indicates that there is some coupling between the rotation rate and number of strakes on the flow stability. As the number of strakes increases, the required rotation rate for a quasistable flow decreases. The yawing moment shows more of a coupling with the side force than the one-strake case did, with the 1000 and 3000 rpm cases showing the best reduction. For both the side force and the yawing moment, the 1000 and 3000 rpm cases show reductions of over 50% from the baseline cases.

The clockwise rotation cases also show similar results as the one-strakes case with the magnitude of the side force (Fig. 16) slightly larger than the baseline case. The yawing moment (Fig. 17) shows magnitudes very similar to those for the one-fin case. The yawing moment follows a similar trend as the side force.

Three Strakes

The results for a slender body with three strakes on a rotating nose tip (Figs. 18–21) show an overall more significant reduction than any of the previous cases with the counterclockwise rotation doing better than the clockwise rotations. Figure 18 shows the side force for the counterclockwise tip with three strakes. The side force is reduced significantly from the baseline for all of the rotation rates. The side force is significantly reduced for rotations of 1000, 3000, and 5000 rpm. Up to about 60 deg, the side force coefficient is within a range of ± 0.75, a reduction of between 80–90%. This is very impressive when compared with the large side forces for the baseline values. Above 60 deg, the rotating nose tip and hence nose tip disturbances have little effect on the vortex formation. The 500 rpm case showed an improved reduction over the two-strake case. For the clockwise rotation case, Fig. 20, the side force is also reduced significantly. Up to 60 deg the coefficient is within the range of ± 1.20. The yawing moments for both the counterclockwise and clockwise rotations show similar magnitudes as for the baseline case, with characteristics similar to the one- and two-strake cases.

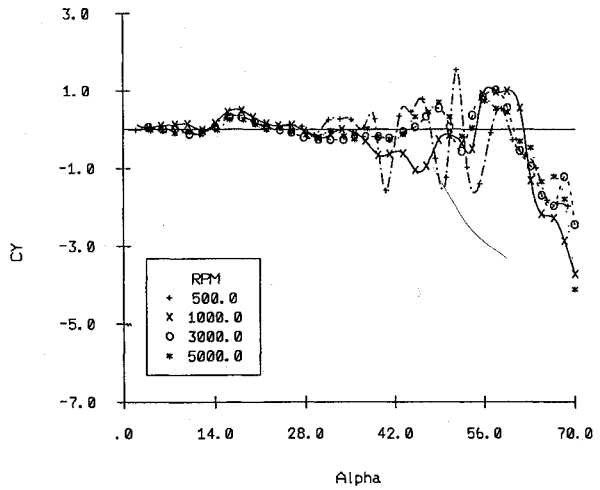

Fig. 18 Side force coefficient for a finless body with three strakes on a counterclockwise rotating nose tip.

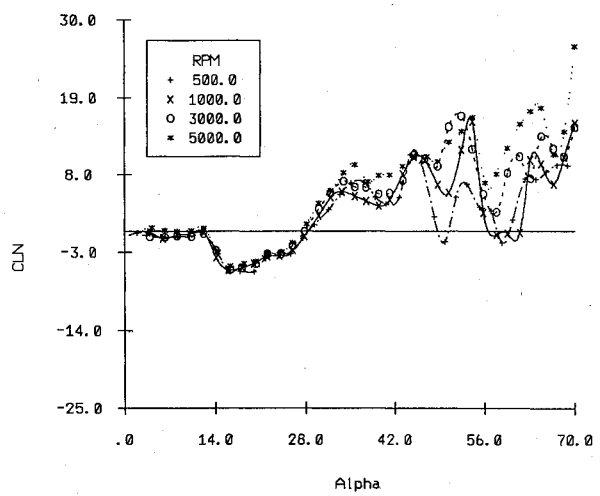

Fig. 19 Yawing moment coefficient for a finless body with three strakes on a counterclockwise rotating nose tip.

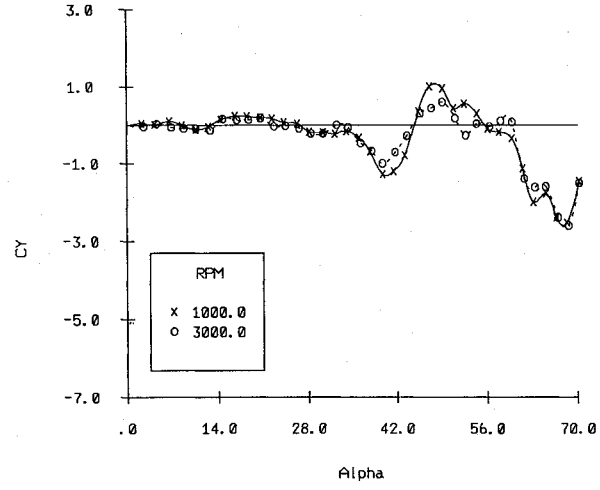

Fig. 20 Side force coefficient for a finless body with three strakes on a clockwise rotating nose tip.

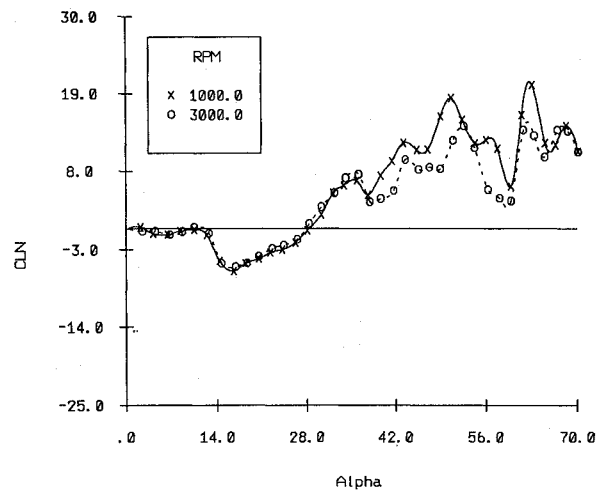

Fig. 21 Yawing moment coefficient for a finless body with three strakes on a clockwise rotating nose tip.

The relationship between the yawing moment and the side force indicates that some tradeoff seems to exist between reduction of the side force and the yawing moment. For cases in which a significant reduction in the side force occurs, the yawing moment (Figs. 19 and 21) generally shows no such reduction.

Flow Instability

Researchers are working to determine the type of instability that occurs on slender bodies at high angles of attack.[15–17] The two types of instabilities that are believed to dominate the flow are convective instabilities and absolute instabilities. The figures showing the side force coefficients may give some insight into these instability types.

The results of Fig. 6 show that all three baseline cases follow a similar trend. The side force remains small for a large range of α and then begins to increase. All of the increases are in the same direction, although the magnitudes are different. At some critical angle (approximately 58 deg) all three curves show significant fluctuations with the angle of attack. The trend is similar for the cases with a counterclockwise spinning nose tip with one strake (Fig. 10). The 500 rpm case apparently does not follow this trend because the rotation rate is too low. The critical angle seems to be shifted to about 45 deg for these cases. The clockwise rotation with one strake on the tip shows similar behavior as Fig. 10, with the critical angle again close to 45 deg. Figures 18 and 20 (three strakes on a rotating nose tip) follow the pattern discussed earlier.

A possible explanation for this behavior is that the flow is dominated by a convective instability through the range of angle of attack until a critical angle is reached where an absolute instability takes over. The behavior of the flow due to each instability is quite different. This behavior explains the random behavior of the curves at higher angles of attack and the ineffectiveness of the rotating nose tip at these higher angles. In the range of convective instability, the nose tip can alter the flow sufficiently to give a reduction in the side force. However, above the critical angle the rotating nose tip shows some reduction but not as great as it shows below that angle.

Summary of Results

Although the results are not presented here, it was observed that the rotating nose tip had very little effect on the normal force and the pitching moment coefficients. The results for the finless body are consistent with published data, and the in-plane forces are consistent with empirical theories.

The baseline case showed that the side force for the slender body had a maximum in the range from 45 to 65 deg angle of attack. Below 45 deg the side force is relatively small. The yawing moment did not necessarily follow the same trends as the side force, sometimes indicating a vortical flow dominated by one vortex in the wake and near the body.

The tests showed a reduction in the side force could be achieved when a rotating nose tip is used. In some cases, a reduction by as much as 80% was observed. However, the percent reduction was dependent upon the number of strakes on the nose tip and the rotation rate. For rotation rates below 500 rpm and above 5000 rpm overall significant reduction was not observed. The range between 1000 and 3000 rpm showed the best characteristics for reduction of the out-of-plane loading.

The general trend showed that the rotating nose tip without strakes showed better performance than a nose tip with either one or two fins. The one- and two-fin cases both showed reduction in the side force from the baseline values. However, the trend showed that as the number of strakes on the nose tip increased, the reduction in the side force also increased. In addition, as the number of strakes increased, the rotation rate played less of a factor. The best reduction in the side force resulted from a rotating nose tip with three strakes and rotating between 1000 and 3000 rpm. Further investigations with more than three strakes on the nose tip would be of interest. The results certainly hint that increased fins may provide additional reduction.

Up to some critical angle of attack the rotating nose tip was shown to give a large reduction in the side force, sometimes as great as 80%. Above this angle, the reduction was not nearly as great or did not always occur. It is speculated that a convective instability governs the asymmetric flow below the critical angle of attack, whereas an absolute instability governs the flow above this angle. Evidence from the side force figures shows that this may be the case.

Conclusions

An array of experiments was conducted on a finless slender body with a fineness ratio of 20.0. The body has a tangent ogive nose of length 2.7 calibers. Four aerodynamic coefficients were measured for each test, but only the side force and yawing moment were presented here. The experiments were done at a Mach number of 0.15 and a Reynolds number of 9.93×10^5.

Wind-tunnel tests show that the use of a rotating nose tip on a slender body can significantly (up to 80%) reduce the side force on the body. The amount of reduction is dependent upon the rotation rate and the number of fins on the rotating nose. There was no significant effect on the reduction of the out-of-plane loading due to the rotation direction. The reduction is greater below some critical angle where the flow may behave with a convective instability. Above the critical angle where an absolute instability may occur, some reduction in the side force takes place, but the reduction is not as significant as below the critical angle.

The results showed that a reduction in the side force did not necessarily give a reduction of the same magnitude in the yawing moment. For the cases where a large reduction in the yawing moment occurred, the side force generally had a magnitude on the order of the baseline value.

References

[1]Deffenbaugh, F. D., and Marshall, F. J., "Time Development of the Flow About an Impulsively Started Cylinder," *AIAA Journal*, Vol. 14, No. 7, 1976, pp. 908–913.

[2]Marshall, F. J., and Deffenbaugh, F. D., "Separated Flow Over a Body of Revolution," *Journal of Aircraft*, Vol. 12, No. 2, 1975, pp. 78–85.

[3]Deffenbaugh, F. D., and Koerner, W. G., "Asymmetric Vortex Wake Development on Missiles at High Angles of Attack," *Journal of Spacecraft and Rockets*, Vol. 14, No. 3, 1977, pp. 155–162.

[4]Meuller, T. J., Nelson, R. C., and Keggelmann, J. T., "Smoke Visualization of Boundary Layer Transition on a Spinning Axisymmetric Body," *AIAA Journal*, Vol. 19, No. 12, 1981, pp. 1607, 1608.

[5]Yanta, W. J., and Wardlaw, A. R., Jr., "Flow Field About and Force on Slender Bodies at High Angles of Attack," *AIAA Journal*, Vol. 19, No. 3, 1981, pp. 296–302.

[6]Mendenhall, M. R., and Lesieutre, D. J., "Prediction of Vortex Shedding from Forebodies with Chines," *Journal of Aircraft*, Vol. 29, No. 3, 1992, pp. 403–412.

[7]Schiff, L. B., Degani, D., and Cummings, R. M., "Computation of Three-Dimensional Turbulent Vortical Flows on Bodies at High Incidence," *Journal of Aircraft*, Vol. 28, No. 11, 1991, pp. 689–699.

[8]Wardlaw, A. B., "Multivortex Model of Asymmetric Shedding on Slender Bodies at High Angles of Attack," AIAA Paper 75-123, Jan. 1975.

[9]Wardlaw, A. B., and Morrison, A. M., "Induced Side Forces at High Angles of Attack," *Journal of Spacecraft and Rockets*, Vol. 31, No. 10, 1976, pp. 589–593.

[10]Gebert, G. A., "Determination of Slender Body Aerodynamics Using Discrete Vortex Methods," *Journal of Spacecraft and Rockets*, Vol. 31, No. 2, 1994, pp. 200–207.

[11]Modi, V. J., and Stewart, A. C., "Approach to Side Force Alleviation Through Modification of the Pointed Forebody Geometry," AIAA Paper 90-2834, Jan. 1990.

[12]Ericsson, L. E., and Reding, J. P., "Alleviation of Vortex-Induced Asymmetric Loads," *Journal of Spacecraft and Rockets*, Vol. 17, No. 6, 1980, pp. 546–553.

[13]Ericsson, L. E., "Unsteady Flow Separation on Slender Bodies at High Angles of Attack," AIAA Paper 90-2835, Jan. 1990.

[14]Ng, T. T., and Malcolm, G. N., "Forebody Vortex Control Using Small, Rotatable Strakes," *Journal of Aircraft*, Vol. 29, No. 4, 1992, pp. 671–678.

[15]Degani, D., and Tobak, M., "Experimental Study of Controlled Tip Disturbance Effect on Flow Asymmetry," *Physics of Fluids*, Vol. 4, Dec. 1992, pp. 2825–2832.

[16]Degani, D., "Effect of Splitter Plate on Unsteady Flows Around a Body of Revolution at Incidence," *Physics of Fluids*, Vol. 3, Sept. 1991, pp. 2122–2131.

[17]Degani, D., "Instabilities of Flows over Bodies at Large Incidence," *AIAA Journal*, Vol. 30, No. 1, 1992, pp. 94–100.

[18]Ericsson, L. E., and Reding, J. P., "Vortex Induced Asymmetric Loads in 2-D and 3-D Flows," AIAA Paper 80-0181, Jan. 1980.

[19]Maynes, R. D., "An Investigation of the Effects of a Rotating Forebody on the Aerodynamics of Slender Bodies at High Angles of Attack," M.S. Thesis, Dept. of Mechanical and Aerospace Engineering, Utah State Univ., Logan, UT, June 1993.

[20]Maynes, R. D., and Gebert, G. A., "An Investigation of the High Angle of Attack Aerodynamics on a Finned and Finless Body with a Fineness Ratio of 20," AIAA Paper 94-0724, Jan. 1994.

[21]Pick, G. S., "Investigation of Side Forces on Ogive-Cylinder Bodies at High Angles of Attack in the $M = 0.5$ to 1.1 Range," AIAA Paper 71-570, June 1971.

[22]Przirembel, C. E. G., and Shereda, D. E., "Aerodynamics of Slender Bodies at High Angles of Attack," *Journal of Spacecraft and Rockets*, Vol. 16, No. 1, 1979, pp. 10–14.

[23]Lowson, M. V., and Ponton, A. J. C., "Symmetry Breaking in Vortex Flows on Conical Bodies," *AIAA Journal*, Vol. 30, No. 6, 1992, pp. 1576–1583.

Jerry Allen
Associate Editor